Unlocking the potential of hidden sites in FAUJASITE: new insights in a proton transfer mechanism

Louwanda Lakiss, Cassandre Kouvatas, Jean-Pierre Gilson, Hristiyan A Aleksandrov, Georgi N Vayssilov, Nikolai Nesterenko, Svetlana Mintova, Valentin Valtchev

Unlocking the potential of hidden sites in FAUJASITE: new insights in a proton transfer mechanism

Louwanda Lakiss,*[a] Cassandre Kouvatas,[a] Jean-Pierre Gilson,[a] Hristiyan A. Aleksandrov,[b] Georgi N. Vayssilov,[b] Nikolai Nesterenko,[c] Svetlana Mintova,[a] Valentin Valtchev*[a]

[a] Normandie Univ, ENSICAEN, UNICAEN, CNRS, LaboratoireCatalyse et Spectrochimie, 14000 Caen, France.
[b] Faculty of Chemistry and Pharmacy, University of Sofia, Blvd. J. Bauchier 1, BG-1126 Sofia, Bulgaria.
[c] Total Research and Technology Feluy (TRTF), Zone Industrielle C, 7181 Feluy, Belgium.

Corresponding authors: louwanda.lakiss@ensicaen.fr, valentin.valtchev@ensicaen.fr

Supporting information for this article is given via a link at the end of the document.

Abstract: Zeolite Y and its ultra-stabilized hierarchical derivative (USY) are the most widely used zeolite-based heterogeneous catalysts in oil refining, petrochemisty, and other chemicals manufacturing. After almost 60 years of academic and industrial research, their resilience is unique as no other catalyst displaced them from key processes such as FCC and hydrocracking. The present study highlights the key difference leading to the exceptional catalytic performance of USY *versus* the parent zeolite Y in a multi-technique study combining advanced spectroscopies (IR and solid-state NMR) and molecular modeling. The set of resultshighlights a hitherto unreported proton transfer involving inaccessible active sites in sodalite cages that contributes to the exceptional catalytic performance of USY.

Introduction

The rare aluminosilicate mineral Faujasite (FAU-type structure) was discovered in 1842.[1]Its synthetic counterpart comprises two different framework compositions, the Y (Si/Al ~ 2.5) and X (Si/Al ~ 1.0) zeolites. A so-called ultra-stable hierarchical derivative of Y, USY (Si/Al ~ 3.0-25), is widely used in oil refining and petrochemistry and holds much promises in biomass upgrading.[2–11] Its introduction in hydrocracking and fluid catalytic cracking (FCC) processes in the early 1960‘s, is a defining moment in heterogeneous catalysis applied to the production of quality transportation fuels and luboils.[12] The importance of FCC and hydrocracking catalysts in the ongoing energy transition will remain as they are also able to process biomass-derived liquids and produce light olefins.[3] Zeolite X, Y, and their derivatives are not only used in industrially relevant catalytic and separation processes but also in emerging applications as nanotechnology, environmental protection, biochemistry, medicine…[13–18]

The three-dimensional FAU structure is built from sodalite cages (cubo-octahedral units of 24 T atoms, *t-toc*) linked by hexagonal prisms (double-six rings of 12 T atoms, *t-hpr*), generating a supercage with a diameter of 1.3 nm.[19] This supercage is accessible through 12 membered ring windows with a diameter of 0.73 nm (Figure S1).[19,20] Zeolite Y develops a high specific surface area (*ca.* 800 m^2g^{-1}) and micropore volume (0.33 cm^3 g^{-1}). Its chemical composition can be easily altered by ion-exchange and other post-synthesis treatments to increase thermal and chemical stability and fine-tune key properties. Such features explain the remarkable resilience of the “first lady” of zeolite catalysis.[3]

Although the FAU-type structure is one of the most open amongst the known zeolites, only a third of its active sites, those located in the supercage, are accessible to reactants.[21–24] The active sites analysis by probe molecules of different size and basicity shows that Brønsted acid located in sodalite cage and hexagonal prism remain inaccessible due to the restricted access through the 6 and 4 member rings windows.[25–27]Noteworthy, the sodalite cage and hexagonal prism are not accessible even to a molecule as small as CO.[26] Therefore, different active sites accessibility must be considered when the FAU zeolite is used as a catalyst.

The post-synthesis transformation of zeolite Y into USY involves a high temperature steaming during which some framework Al is expelled to extra-framework (EFAl) positions and replaced by Si via a T-jump mechanism, decreasing the number of accessible Brønsted active sites.[27] This atomic reshuffling also generates a hierarchical material by adding mesopores to the native zeolite microporosity.[11,27] Although USY contains far fewer active sites than its Y parent, it exhibits a much higher catalytic activity.[28,29] Numerous studies attribute this superior performance to a synergy between the extraframework aluminum species (EFAl) generated during steaming[29–31] and vicinal Brønsted acid sites. This intimate interaction creates so-called enhanced or highly reactive acidic sites. Even though several papers reported that EFAl species increase some hydrocarbons (i-C_4H_{10},[30]n-C_5H_{12},[32] and n-C_6H_{14}[33]) cracking rates, they all failed to find a direct correlation between these species and the catalytic activity. Gounder *et al.* proposed that the presence of EFAl increased the confinement of reactants by decreasing the effective size of the supercage.[34] However, the EFAl, comprising mostly highly polymerized aluminum oxides, are either preferentially located on the USY external surface or often removed by acid washing. For instance, the widely studied commercial USY from Zeolyst, CBV760, contains few

EFAl (Lewis acid sites), typically less than 0.1 mmol/g, although they display a higher catalytic activity than its Y parent.[23] In a nutshell, the fundamentals of such an unexpectedly high catalytic activity in USY are still debated after about 60 years of academic research and impressive commercial successes.

Answering this question is essential to design superior Y zeolites, able to meet the current and emerging catalytic challenges in the ongoing energy, environmental and chemical transition.

We recently reported that a novel chemical treatment, the unbiased leaching of framework Si and Al by a NH_4F solution, could open some sodalite cages in Y zeolite.[35] Our starting hypothesis is that partial destruction of some sodalite cages in zeolite Y might also occur during the steaming process leading to its USY derivative. Herein, a combination of advanced spectroscopic techniques and molecular modeling is employed to investigate the structural and chemical changes occurring during the USY zeolite preparation and thus to highlight the origin of its unique properties.

The accessibility of the active sites in the supercage and sodalite cage, is investigated by infrared spectroscopy using probe molecules with different kinetic diameters (∅) and proton affinities (PA) - CO (∅=0.38 nm, PA=598 kJ/mol), pyridine (∅=0.57 nm, PA=912 kJ/mol) and 2,6-Di-tertbutylpyridine (∅=0.83 nm, PA=983 kJ/mol).[27] The interactions between these probes and the zeolites are further investigated by solid-state NMR spectroscopy and density functional theory (DFT) modeling.

Results and discussion

Highly crystalline samples of zeolite Y and USY were used in this study (Figure S2). The physicochemical properties of two zeolites are presented in Table 1. The major differences between Y and USY zeolites are the presence of mesopores and a much higher Si/Al ratio of the latter. The mesoporosity of USY is a consequence of partial destruction of the zeolite framework, including the sodalite cages, during the steaming procedure, followed by acid leaching of extra framework aluminum.

Table 1. Physico-chemical properties of employed zeolite Y and USY samples.

Zeolite	U.C. (Å)[a]	Si/Al [b]	V_{Micro} (cm^3/g) [c]	S_{BET} (m^2/g) [c]	S_{Meso} (m^2/g) [c]	Brønsted sites (mmol/g) [d]	Lewis sites (mmol/g) [d]
Y	24.7	2.3	0.34	754	60	1.30	0.04
USY	24.2	28	0.27	805	261	0.24	0.08

[a]refined unit cell parameter;[b]determined by deconvolution of ^{29}Si MAS NMR spectra;[c]determined by nitrogen sorption analyses;[d]determined by pyridine adsorption $\varepsilon_{Brønsted}$ at 1550 cm^{-1} =1.35 $cm.\mu mol^{-1}$, ε_{Lewis} at 1450 cm^{-1}=1.5 $cm.\mu mol^{-1}$.(see supporting information for nitrogen sorption analyses and pore size distributions).

Spectroscopic study

Infrared spectroscopy

Figure 1A shows the hydroxyls stretching vibration (4000-3000 cm^{-1} window) after CO adsorption to saturation (T = 100 K) on zeolite Y. The corresponding CO stretching (2250-2000 cm^{-1}) is reported in Figure S3A. Upon CO adsorption, the band associated with the bridged hydroxyls located in the supercage (OH_{Super}) at 3650 cm^{-1} is shifted to 3350 cm^{-1} due to its interaction with CO, while those in sodalite cages (OH_{Sod}: 3540 cm^{-1}) are unaffected. The acid site concentrations of the OH_{Super} and $OH_{Sod,}$ as well as the OH_{Super} interacting with CO, are summarized in Table 2. The amount of tetrahedral aluminum (Al^{IV}), calculated from the Si/Al ratio determined by ^{29}Si MAS NMR, provided the total number of acid sites (OH_{Super} and OH_{Sod}). In Y, the numbers of acid sites determined by quantifying the bridged hydroxyls (OH_{Super} + OH_{Sod} = 3.40 mmol/g) and the tetrahedral aluminum (Al^{IV} = 3.56 mmol/g) were very close. In USY, the number of bridged hydroxyls determined by IR is only 60 % of the value derived from ^{29}Si NMR due to partial amorphization (30%) and steaming.[36] The spectral evolution of USY interacting with CO (Figure 1B and Figure S3B) is similar to that of Y zeolite, *i.e.,* only OH_{Super} are accessible, and the associated band shifts to 3275 cm^{-1}. The low-intensity band at 3670 cm^{-1} corresponds to extraframework -(AlOH)- species.[37,38] The total acidity probed by CO is very close to the number of OH_{Super}. This confirms again that, despite its small size, CO does not interact with OH_{Sod} in both Y and USY zeolites. The stretching band of OH_{super} shifts upon CO adsorption ($\Delta\nu$OH) on Y (300 cm^{-1}) and USY (360) (Figure 1), while the associated stretching bands of adsorbed CO ($\Delta\nu$CO) are 35 cm^{-1} and 40 cm^{-1} (Figure S3). As $\Delta\nu$CO is indicative of the acid strength of the corresponding O-H[16], the acid sites (OH_{Super}) in USY appear stronger than those of zeolite Y.

It is not surprising that CO (kinetic diameter 0.38 nm) cannot access the sodalite cage of zeolite Y through the 0.28 nm 6MR window. However, for USY, it is somewhat surprising that even after partial destruction of the framework, CO cannot access a portion of sodalite cages.

DFT modeling is used to further elucidate this inaccessibility; more methodological details are available in the supporting information. For USY, we consider models with two and four T-atom vacancies (Figures S4A, B) occupied by hydrogen-bonded silanols (nests), preventing adsorbates from entering the sodalite cage. Each model contains a Brønsted acid site with the acidic proton oriented towards the sodalite cage and the hexagonal prism; thus it is not accessible from the adjacent supercage. One may assume that after removal of silicon centers from the hexagonal prism and formation of silicon vacancies, the acidic proton will be accessible for the guest molecules(Figures S4C, D). However, even in the

four T-atoms vacancies model (Figure S5), probe molecules cannot interact directly with the OH_{Sod} and therefore be polarized or protonated. The reason for this is the blocking of the access to the bridging OH_{Sod} group by the silanols - the interatomic distance between the oxygen atoms of the first group of silanols, close to the supercage, is in the range 0.48 – 0.50 nm, which is sufficiently large the Py molecule to enter (the sum of VDW radia of two O and N is 0.46 nm), but the distance between oxygens of the second group of silanols is too short, 0.42 – 0.44 nm, for Py to enter. The same is valid for the CO molecules, for which the sum of the VDW radia is 0.47 nm. This modeling fits well with the experimental data of CO adsorbed on USY zeolite; it calculates that the presence of silanol nests reduces the E_{deprot} of bridge hydroxyls by 23 kJ/mol (more in SI). Thus, when a silanol nest is close to a bridging OH, the latter's acidity increases, in good agreement with the shifts of 360 cm^{-1} for the OH_{Super} ($\Delta\nu$ OH) and 40 cm^{-1} for CO ($\Delta\nu$CO) vibrations upon CO adsorption on a Y and USY, *vide supra*.

Table 2.Framework Al (^{29}Si NMR spectroscopy) and acid site concentrations (IR spectroscopy) for Y and USY zeolites.

Zeolite	Al^{IV} mmol/g[a]	OH_{Super} mmol/g [b]	OH_{Sod} mmol/g [b]	OH^{CO} mmol/g [c]	OH^{PY} mmol/g [d]	$OH^{2,6DTBPy}$ mmol/g[d]
Y	3.56	1.30	2.10	1.10	1.30	1.20
USY	0.52	0.14	0.18	0.10	0.24	0.26

[a] Tetrahedral (framework) aluminum calculated from the Si/Al ratio determined by ^{29}Si MAS NMR[23]

[b] OH in supercage and sodalite cage determined using the molar absorption coefficients of the respective OH bands[39]

[c]OH probed by CO using the molar absorption coefficient of the CO-OH band at 2172 cm^{-1}[16]

[d] OH probed by pyridine and 2,6-di-tert-butylpyridine using the molar absorption coefficient of their protonated band at 1545 cm^{-1} and 3360 cm^{-1}respectively[23]

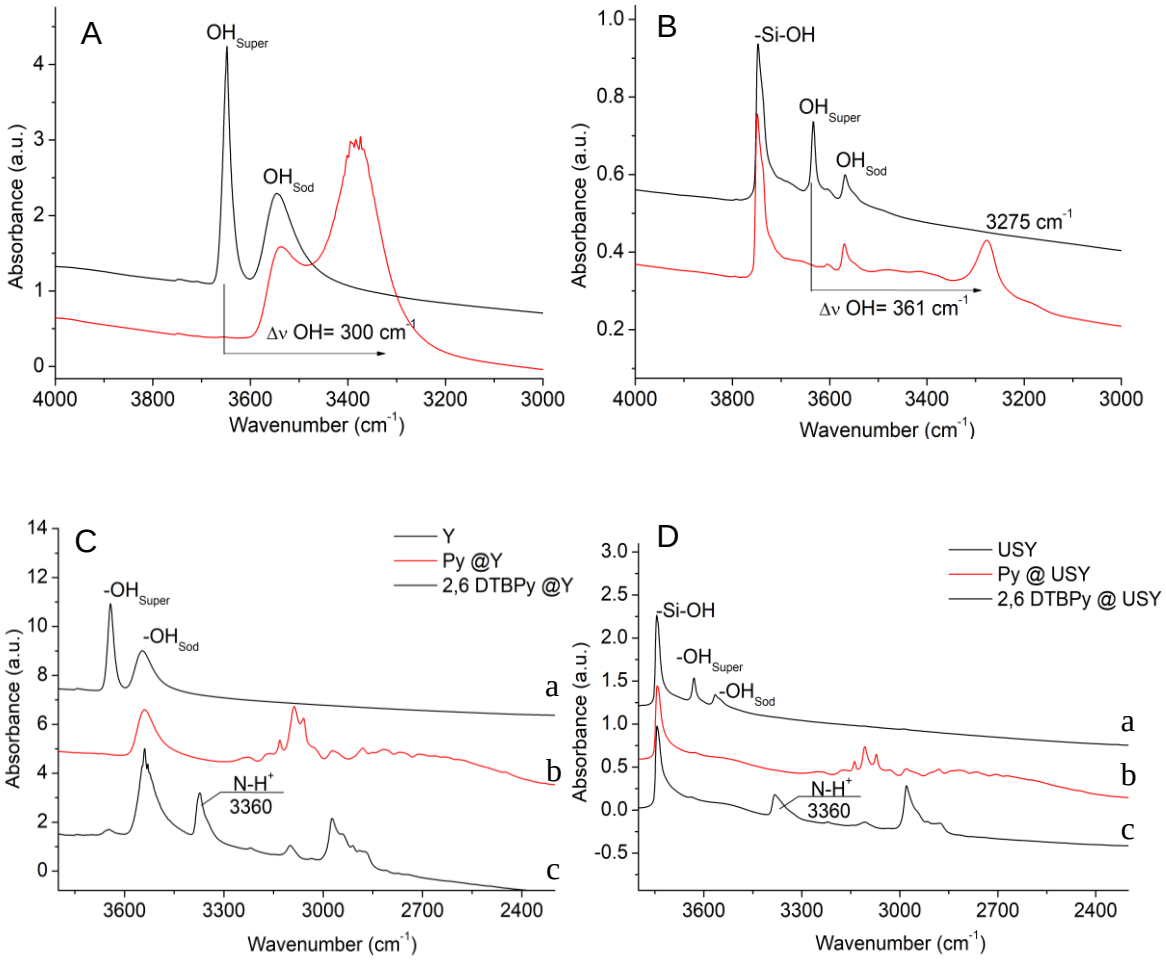

Figure 1. IR spectra in the OH window of Y (A) and USY (B) zeolites after (a) activation at 723 K and (b) CO adsorption at 100 K. IR spectra of Y (C) and USY (D) after (a) activation at 723 K, (b) adsorption of Py and evacuation at 423 K under secondary vacuum, and (c) adsorption of DTBPy and evacuation at 423 K under secondary vacuum.

Upon adsorption of Py and DTBPy, the OH_{super} bands disappear gradually in both zeolites (Figures 1C, D). However, the OH_{Sod} in Y and USY behave differently. Py and DTBPy do not interact with the OH_{Sod} in Y (Figure 1C) as the 3540 cm^{-1} band remains intact after either Py or DTBPy adsorption after evacuation at 423 K. A weak partial interaction of OH_{Sod} with pyridine (a small negative peak at 3562 cm-1 and a broadening of the peak appear in the difference spectrum (Figure S12) is observed. The amount of these probes protonated on Y is in line with the concentration of OHSuper as well as all OH titrated by CO (Table 2). In agreement with this result, DFT modeling indicates that on Y zeolite, pyridine and 2,6-di-tertbutylpyridine are protonated only by the acidic OHSuper with binding energies of -168 kJ and -222 kJ/mol, respectively (Table S1). On the other hand, upon Py and DTBPy adsorption on USY, the OH_{Sod} band disappears, indicating a strong interaction between these probes and OH_{Sod}, Figure 1D. Moreover, the number of acidic sites probed by Py and DTBPy is close to the sum of OHSuper and OH_{Sod}, Table 2. The fraction of Py (0.14 mmol/g) and DTBPy (0.16 mmol/g) interacting with OH_{Sod}, is calculated and in good agreement with the amount of OH_{Sod} calculated by integrating its corresponding band (3540 cm^{-1}) intensity. Py and DTBPy would therefore be protonated by Brønsted acid sites located in the USY sodalite cages. To evaluate the validity of the results obtained on CBV760 we have studied two more USY samples, CBV712 (Si/Al=7) and CBV720 (Si/Al=16). Similar behavior has been observed for all USY samples, no matter of different Si/Al ratios. Both the OH_{Super} and OH_{Sod} disappeared after pyridine adsorption (Figure S14).This is, at first glance, surprising since both molecules cannot penetrate sodalite cages.[40] Moreover, flipping all OH_{Sod} in the supercage to reach Py and DTBPy is impossible due to the crystalline framework's rigidity.[16] Indeed, proton flipping or jumping between two oxygen atoms surrounding the aluminum (first coordination sphere) might occur, but it is an isolated phenomenon that involves only a few of the OH situated in the sodalite cage. Proton mobility or

proton hopping in zeolites was already investigated by several groups using temperature-dependent 1H NMR spectroscopy, temperature-dependent infrared spectroscopy, DFT and ab Initio calculations.[41–45] For instance, Sierka and Sauer[44] studied the dynamics of Brønsted acidic sites in MFI (ZSM-5), CHA (SSZ-13) and FAU (Y) zeolites by ab initio calculations and demonstrated that proton jumps occur in FAU and CHA structures, but to a lower extent than in ZSM-5. Such a mechanism is highly dependent on the flexibility of the structure and the temperature. They also concluded that this tunneling effect is negligible at temperatures above room temperature. Hence, a proton transfer between an acidic OH_{Sod} and a bulky probe molecule in USY should occur by an as yet unreported mechanism since a direct proton jump is impossible.

DFT modeling of the interaction between Py and DTBPy with USY could provide insights to the protonation mechanism. A structural model with one Al center (generating an inward-looking bridging hydroxyl in the sodalite cage, OH_{Sod}) and two nearby T-atom vacancies is considered together with three states of the basic probes: (1) unprotonated (initial state), (2) protonated by one of the silanols near the bridging hydroxyl (intermediate state), and (3) a proton from the bridging hydroxyl is transferred to restore the neighboring silanol group (Figure 2). In such a scenario, the Brønsted acid site protonates the basic probe *via* a two-step proton transfer (*aka* proton shuttle). The binding energies of DTBPy of complexes 1, 2 and 3 are -65, -112 and -246 kJ/mol (Table S1 in SI), thus, the two steps of the proton transfer are exothermic by 47 kJ/mol and 134 kJ/mol, respectively. The same trends are found for Py protonation. The calculated Gibbs free energies of different complexes (Table S1) also suggest that the protonation of DTBPy is favorable with ΔG values of -39 and -126 kJ/mol for the first and for the second step, respectively. In addition, we searched for transitions states of the proton transfer and the calculated activation barriers for the two steps are 2 and 65 kJ/mol. One may note that DTBPy protonation by the silanol is essentially barrier less since it is easily accessible for nitrogen atom of the base molecule, while the second step requires more distant proton transfer from the bridging hydroxyl to the deprotonated silanol. In any case, the low values suggest that the proton transfer via the proton shuttle mechanism mediated by silanol group occurs easy.

A model with four T-atom vacancies will accommodate a larger nest with 8 silanols (Figure S5). However, neither Py nor DTBPy can enter the sodalite cage since the silanol nest blocks its entrance, as described above. The Py and DTBPy basicities are sufficiently high to allow their protonation by a silanol from the nest. The binding energies of the protonated Py and DTBPy are -107 kJ/mol and -113 kJ/mol, respectively; in turn, the acidity of the corresponding silanol from the nest is enhanced since the remaining silanols stabilize the deprotonated oxygen by H-bonding.The calculated Gibbs free energies for the Py and DTBPy models protonated by the silanol nests are -60 and -60 kJ/mol, i.e. the protonation process is exergonic with respect to the sorption energy of molecules before protonation, 12 and -23 kJ/mol, respectively (Table S1 of SI).

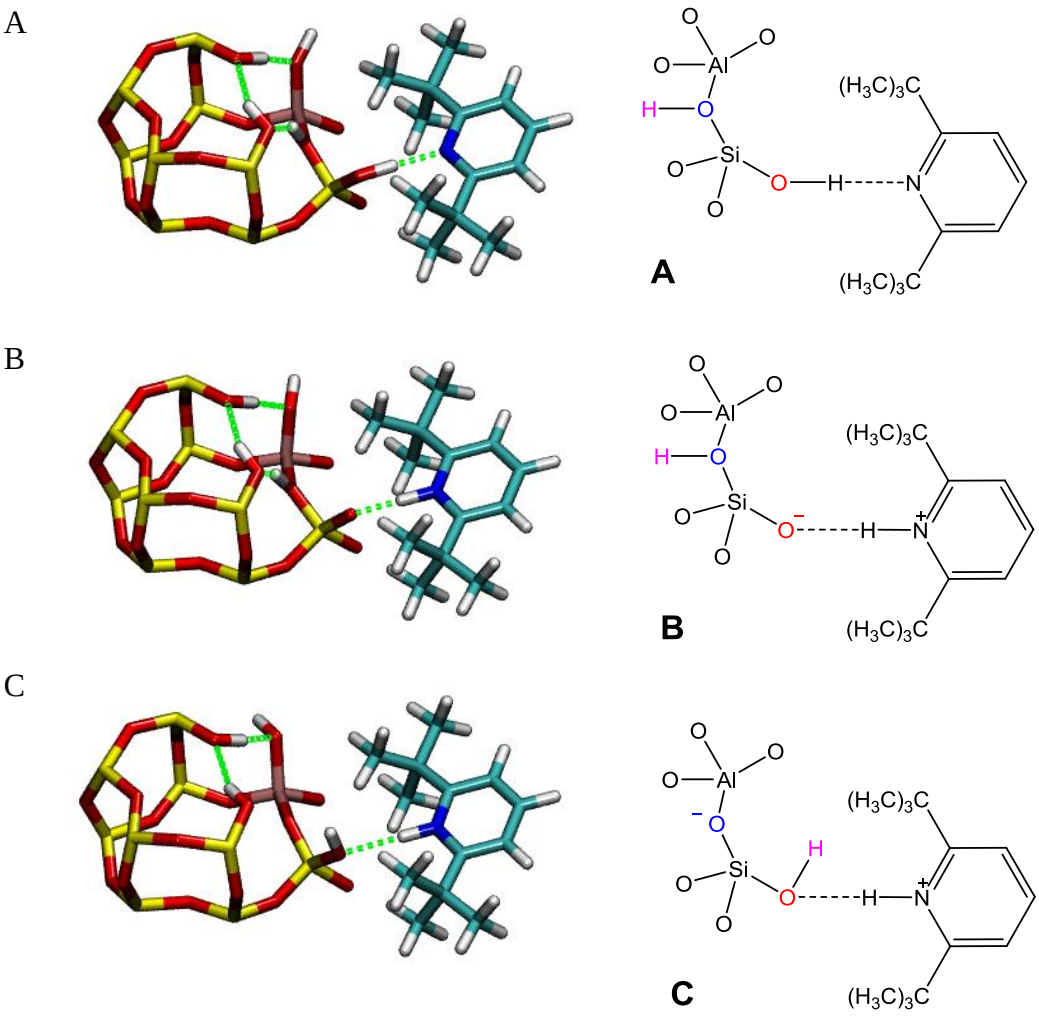

Figure 2. Local structure showing the proton transfer from bridging OH group to 2,6-di-tertbutylpyridyne via one silanol: initial unprotonated state (A), protonated by the silanol (B), proton from the bridging OH group transferred to restore the silanol group (C).Fragments of the optimized structures shown in the left column are presented as structural formula in the right column.

The model that best fits the IR results is one with two T-atom vacancies near a Brønsted acid site: Py and 2,6-DTBPy are protonated by a proton transfer via a silanol. The initial proton is taken from a silanol, and the deprotonated oxygen then accommodates a proton transferred from the most acidic bridging hydroxyl group inside the sodalite cage (Figure 3). The increased flexibility of the zeolite framework near the T vacancy also facilitates a partial reorientation of this bridging hydroxyl.

Both, DFT modeling and IR spectroscopy,points out that a proton transfer occurs when a few T atoms are replaced with bridging hydroxyls. Figure 3 illustrates the proton transfer mechanism from the sodalite cage to the supercage when a probe molecule is in close proximity. The protonation through a “gate-keeper” silanol is followed by a proton transfer from a Brønsted site located in the sodalite cage to restore the silanol. In that way, the Brønsted acid site in the sodalite cage is indirectly involved during a chemical reaction. As a result, a substantial fraction of the Brønsted acid sites located in the USY sodalite cage, spectators in a conventional zeolite Y, could participate and contribute to the chemical reaction.

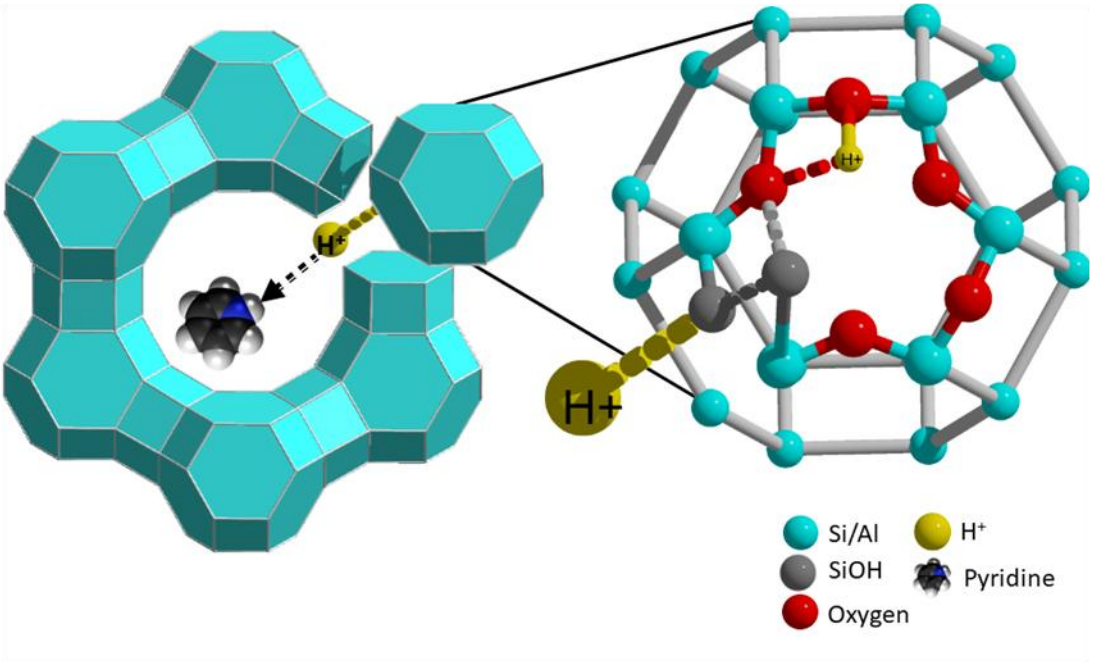

Figure 3. Proton transfer mechanism in a USY sodalite cage: A) FAU framework viewed along [111], B) Sodalite building unit (for clarity only the oxygen atoms in the highlighted hexagonal facet are represented) with the proton transfer via a silanol nest.

NMR spectroscopy

Solid-state NMR is frequently used in conjunction with IR to probe the local structure of zeolites and their hydroxyls in particular. In this study, we combined several NMR techniques to shed more light on the proton transfer in USY revealed by the IR and modeling studies.

^{1}H MAS NMR spectroscopy

In the ^{1}H MAS NMR spectrum of USY (Figure S6), four distinct signals appear at 1.9 ppm (H1), 3.2 ppm (H2), 4.5 ppm (H3), and 6.5 ppm (H4). H1 is commonly assigned to external or internal silanols while H2 and H3 correspond to Brønsted acid sites located in supercage and sodalite cage, respectively.[46–49] H4 corresponds to acid sites with enhanced acidity tentatively associated with isolated Brønsted sites (AlOHSi).[50] In our case, H4 is not related to any ammonium residue as the {^{1}H}-^{15}N CP NMR spectrum does not show any ammonium cations, in agreement with the zeolite IR spectrum where the characteristic deformation vibration band of ammonium at 1455 cm^{-1}is absent, Figure S7.[16]The remaining signal at 2.6 ppm corresponds to extraframework aluminum species H_{EFAL}.

^{1}H-{^{27}Al } TRAPDOR MAS NMR (TRAnsfer of Population in DOubleResonance)

^{1}H-{^{27}Al } TRAPDOR MAS NMR[51] distinguishes between internal and external silanols by resolving the H1 (1.9 ppm) signal into two distinct ones H1' (internal silanols, 2 ppm) and H1'' (external silanols, 1.8 ppm).(Figure S8) Since silanol peaks are impacted by ^{27}Al irradiation during the TRAPDOR experiment, they should be close to Al species (see SI). This closeness is further highlighted by a Back-to-Back (BABA) SQ-DQ ^{1}H-^{1}H spectrum (Figure 4A), probing spatial proximities between hydrogen species through correlations reported in Table S2. Internal silanols are spatially close to acidic OH in both environments (OH_{Sod} and OH_{Super}), in turn, close to each other. In addition, Brønsted acid sites in the supercage are near EFAL species but also close to acidic OH hydrogen-bonded to neighboring framework oxygen. Since the BABA sequence probes distance in the 2-3 Å range, H4 can be attributed to the H bonding of an acidic OH_{Super}.

Proton mobility probed by ^{1}H-^{1}H magnetization exchange

To investigate the proton transfer mechanism revealed by the IR and modeling studies, the ^{1}H-^{1}H magnetization exchange in USY is monitored at mixing times of 5, 50, and 500 ms. (Figures 3B-D) The off-diagonal peaks (cross-peaks) usually originate from spin diffusion or chemical exchange between close ^{1}H spins. However, such magnetization transfer between ^{1}H species can also occur at longer distances when mobile species, like water, are involved. As our experiments are performed on dried samples (see Experimental section), the cross-peaks are not due to mobile water.

Cross correlations of the magnetization exchange are reported in Table 3. At a short mixing time of 5 ms (Figure 4B), no cross-peaks appear since spin diffusion does not occur with such a short mixing time. At 50 ms (Figure 4C), a strong cross-peak appears between silanols and acidic OH_{Sod} indicating exchange between these two sites, *i.e.,* their spatial proximity already highlighted in the BABA experiment, *vide supra*. With a 500 ms mixing time, a second cross-peak appears between silanols and isolated Brønsted acid sites. (Figure 4D). The long time scale (500 ms) required to observe this cross-peak implies a rather slow exchange between these species, relatively distant from each other as no corresponding cross-peak appears in the BABA spectrum.

^{1}H-^{1}H magnetization exchange in combination with BABA experiments prove that internal silanols are spatially close to acidic OH_{Sod}, favoring the proton exchange observed at the 50 ms mixing time. Moreover, CP {^{1}H}-^{29}Si MAS **(**Figure S9) and 2D CP HETCOR {^{1}H}-^{29}Si (Figure S10) experiments performed with contact times of 7.5 and 1 ms concur with this hypothesis. Indeed, combining ^{29}Si MAS, {^{1}H}^{29}Si CPMAS and 2D {^{1}H}^{29}Si HETCOR MAS NMR confirms i) the existence of Q^4 species close to Brønsted acid sites in sodalite cages, and ii) a spatial proximity between some of them and SiOH species. These conclusions are also in agreement with BABA experiments indicating that silanols are spatially close to acidic OH_{Sod}.

Table 3. Cross-correlation (in ppm) in the ^{1}H^{1}H magnetization exchange experiment, with corresponding hydrogen species, for 5 ms, 50 ms, and 500 ms mixing times.

Mixing time (ms)	Cross-correlations / ppm	Corresponding Hydrogens	Hydrogen species
5	No correlation	-	-
50	(1.9;4.5)	H1 / H3	SiOH / OH_{Sod}
500	(1.9;4.5)	H1 / H3	SiOH / OH_{Sod}
	(1.9;6.5)	H1 / H4	SiOH / hydrogen-bonded acidic OH_{Super}

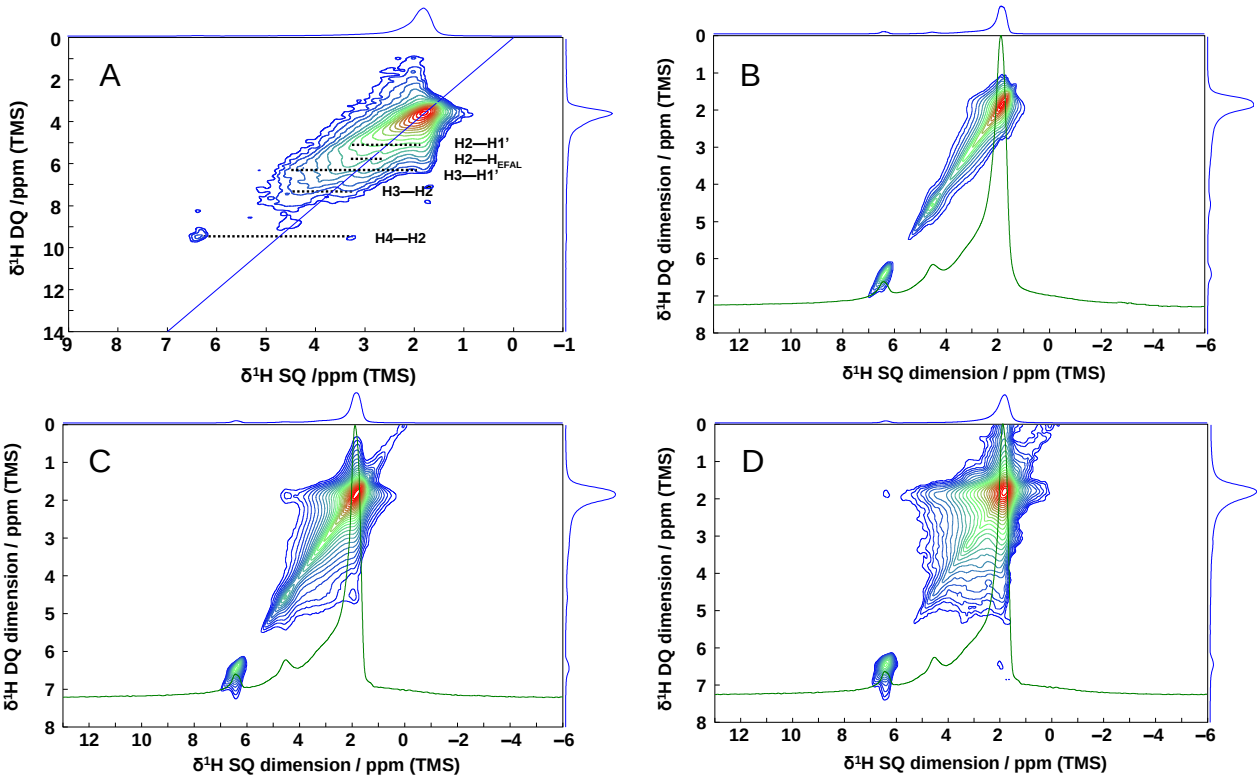

Figure 4. (A)1H-1H SQ-DQ BABA spectrum of USY zeolite dried at 200°C for 12 h. The dotted horizontal lines highlight a correlation, verified by the extraction of corresponding slices of the direct dimension. 1H-1H magnetization exchange spectra of USY zeolite dried at 200°C for 12 h, with mixing times of (B) 5 ms, (C) 50 ms, and (D) 500 ms.

Discussion

The experimental data show that the unique properties of USY zeolite *vs* its parent sample (FAU-Y) result from several inter-related structural modifications that lead to a new property altering the catalytic performance. First, the common supercage acid sites OH_{Super} present in both samples, Y and USY, are stronger in USY. This was confirmed by CO adsorption and modeling. It is also well known[52] that zeolites bridged acid sites strength increases when the Si/Al ratio increases. As confirmed by infrared and NMR experiments, the OH_{Sod}, which are spectators in FAU-Y becomes accessible to probe molecules in USY via the proton transfer mechanism demonstrated above. Indeed, the presence of silanols next to Brønsted acid sites in the USY zeolite provides several advantages. It increases the accessibility of USY *vs* FAU-Y, toward sterically hindered molecules, as it was observed for Pyridine and 2,6-Di-tertbutylpyridine. Even if a bridging hydroxyl from the sodalite cage points to the supercage, it will remain embedded in the rigid zeolite framework, rendering molecule's protonation more difficult and therefore slower. On the other hand, a silanol, in which the hydroxyl oxygen is bound to only one T-atom, is more mobile than the oxygen from a bridging hydroxyl, which is fixed with covalent bond between two T-atoms of the zeolite framework (this can be confirmed by the higher value of the calculated bending mode of the oxygen from bridging hydroxyl, 250 cm^{-1}, compared to the value for the oxygen from silanol hydroxyl, 157 cm^{-1}). Such a hydroxyl is, therefore, easier to access by a basic guest. This is illustrated by comparing the computed distance between the DTBPy nitrogen and the oxygen from the proton donating hydroxyl: 312 pm for adsorption on a 'classical" bridging hydroxyl in the Y zeolite supercage *vs* 274 pm in the defect structure of USY, *i.e.*, about 40 pm closer (Figures S4E, F). This favorable interaction with an acid site is important not only to protonate basic probe molecules but also for reactants (Figures 2 and 3) during the catalytic reaction. The NMR study clearly showed that contrariwise to FAU-Y, USY display extremely high acidic sites (H4 sites) that might correspond to isolated Brønsted sites (AlOHSi).[50] These acid sites are absent in FAU-Y. The effect of shortening (internal) the diffusion pathlengths, *i.e.*, the additional mesoporosity introduced during stabilization, is also present, but it is not the major factor for this high performance. To exclude this possibility a homemade nanosized zeolite, nano-Y (70 nm particle size, referred to Y-70 in the original report),[53] with a similar framework (Si/Al = 1.7) composition is tested in a model catalytic reaction (isooctane cracking) under identical conditions. The isooctane conversion on USY is 7-10 times higher than its Y parent, while on nanosized Y the conversion is only twice higher. (Figure S11) Thus, as expected, the exceptional catalytic activity of USY zeolite is therefore not due to a shortened diffusion pathlength of the reactant. It results from the combined activity of three types of active sites different in nature, in strength, and location. At the same time, the catalytic activity of FAU-Y is only due to the activity of its accessible OH_{Super}.

Conclusions

We show that in the USY zeolite, three different types of active sitesparticipatein the protonation of guest molecules (basic probes and reactants) and are responsible for its superior catalytic cracking activity. During the steaming of zeolite Y to produce USY, mesopores are created by partial framework destruction, including a fraction of the sodalite cages. The missing T atoms are replaced by silanol nests acting as gatekeepers preventing access of molecules, even CO, inside the sodalite cages. As a result, a direct proton transfer from a Brønsted site in the sodalite cage cannot reach a basic probe molecule or a reactant.

A combined IR - NMR spectroscopy coupled with DFT molecular modeling reveals a new, as yet unreported, proton transfer mechanism in USY involving a Brønsted acid site located in a sodalite cage (OH_{Sod}). So far, reputedinaccessible acid sites, located in sodalite cage partially opened, now contribute to protonate molecules confined in the supercage. This explains the superior catalytic cracking activity of USY *via* a proton transfer process to the silanols gatekeepers.

These findings allow a better understanding of the *modus operandi* of the all-important USY-based catalysts, an already key catalyst in oil refining and petrochemistry. This will lead, in turn, to a more efficient fine-tuning of the catalytic properties of the FAU structure. As this structure is only a member of the family of cage-containing zeolites (LTL-, LTA-, CHA-, RHO…) these could also benefit from this new option to boost or better adjust their catalytic or other performances.

Acknowledgments

The authors acknowledge the financial support from the Industrial Chair ANR-TOTAL “NanoClean Energy” (ANR-17-CHIN-0005-01) and FEDER 18P01675. HAA is grateful for support from Bulgarian ScienceFund (contract KP-06-DO02/2), GNV acknowledges the support of the project EXTREME, funded by the Bulgarian Ministry of Education and Science, D01-76/30.03.2021, programme “European Scientific Networks”.

Keywords: Zeolite • Faujasite • Supercage • Brønsted acid sites • Sodalite

Author contributions

V.V. and L.L. led the overall design and direction of the project. L.L. performed the catalytic and IR experiments; C.K. performed the NMR studies; H.A.A. and G.N.V. performed the molecular modelingand participated in the analysis of the results. J-P.G., S.M. and N.N. participated in the analysis and discussion of experimental results. L.L., J-P.G. and V.V. prepared the manuscript with help from all authors.

[1] W. Bergerhoff, G. Baur, W.H. Nowacki, *N. Jb. Miner. Mh.***1958**, 193–200.
[2] W. Vermeiren, J.-P. Gilson, *Top. Catal.***2009**, *52*, 1131–1161.
[3] E. T. C. Vogt, B. M. Weckhuysen, *Chem. Soc. Rev.***2015**, *44*, 7342–7370.
[4] A. De Klerk, *Molecules***2018**, *23*, 1–17.
[5] M. S. Rigutto, R. van Veen, L. Huve, *Zeolites in Hydrocarbon Processing*, Elsevier B.V., **2007**.
[6] S. Kulprathipanja, *Zeolites in Industrial Separation and Catalysis*, Wiley-VCH, Weinheim, Germany, **2010**.
[7] T. Ennaert, J. Van Aelst, J. Dijkmans, R. De Clercq, W. Schutyser, M. Dusselier, D. Verboekend, B. F. Sels, *Chem. Soc. Rev.***2016**, *45*, 584–611.
[8] E. M. Flanigen, R. W. Broach, S. T. Wilson, in *Zeolites Ind. Sep. Catal.*, John Wiley & Sons, Ltd, **2010**, pp. 1–26.
[9] M. Guisnet, J.-P. Gilson, *Zeolites for Cleaner Technologies*, Imperial College Press, London, **2003**.
[10] C. Martínez, A. Corma, *Coord. Chem. Rev.***2011**, *255*, 1558–1580.
[11] D. Verboekend, N. Nuttens, R. Locus, J. Van Aelst, P. Verolme, J. C. Groen, J. Perez-Ramırez, B. F. Sels, *Chem. Soc. Rev.***2016**, *45*, 3331–3352.
[12] C. Marcilly, D. Decroocq, *Acido-Basic Catalysis : Application to Refining and Petrochemistry*, Éd. Technip, Paris, **2006**.
[13] M. P. Pina, R. Mallada, M. Arruebo, M. Urbiztondo, N. Navascués, O. De La Iglesia, J. Santamaria, *Microporous Mesoporous Mater.***2011**, *144*, 19–27.
[14] S. Mintova, M. Jaber, V. Valtchev, *Chem. Soc. Rev.***2015**, *44*, 7207–7233.
[15] J. D. Sherman, *Proc. Natl. Acad. Sci. U. S. A.***1999**, *96*, 3471–3478.
[16] O. Cairon, T. Chevreau, *J. Chem. Soc. Faraday Trans.***1998**, *94*, 323–330.
[17] Y. Shi, S. Ye, H. Liao, J. Liu, D. Wang, *J. Solid State Chem.***2020**, *285*, 121227–121232.
[18] E. Kontogiannidou, C. Karavasili, M. G. Kouskoura, M. Filippousi, G. Van Tendeloo, I. I. Andreadis, G. K. Eleftheriadis, I. Kontopoulou, C. K. Markopoulou, N. Bouropoulos, D. G. Fatouros, *J. Drug Deliv. Sci. Technol.***2019**, *51*, 177–184.
[19] “FAU: Framework Type,” can be found under https://europe.iza-structure.org/IZA-SC/framework.php?STC=FAU.
[20] J. A. Kaduk, J. Faber, *Rigaku J. 14***1995**, *12*, 14–34.
[21] J. Van den Berg, J. Gascon, F. Kapteijn, in *Zeolites Catal.* (Ed.: Z.S. Cejka, Jiri, Corma, Avelino), Wiley-VCH, Weinheim, **2010**, pp. 361–387.
[22] N. Y. Chen, T. F. Degnan Jr., C. Morris Smith, *Molecular Transport and Reaction in Zeolites: Design and Application of Shape Selective Catalysis,* Wiley, **1994**.
[23] L. Lakiss, A. Vicente, J. P. Gilson, V. Valtchev, S. Mintova, A. Vimont, R. Bedard, S. Abdo, J. Bricker, *ChemPhysChem***2020**, 1873–1881.
[24] T. Frising, P. Leflaive, *Microporous Mesoporous Mater.***2008**, *114*, 27–63.
[25] W. H. Baur, *J. Am. Miner.***1964**, *49*, 697–704.
[26] W. Daniell, N. Y. Topsøe, H. Knözinger, *Langmuir***2001**, *17*, 6233–6239.
[27] S. Van Donk, A. H. Janssen, J. H. Bitter, K. P. De Jong, *Catal. Rev. - Sci. Eng.***2003**, *45*, 297–319.
[28] K. Okumura, T. Tomiyama, N. Morishita, T. Sanada, K. Kamiguchi, N. Katada, M. Niwa, *Appl. Catal. A Gen***2011**, *405*, 8–17.
[29] J. R. Sohn, S. J. DeCanio, P. O. Fritz, J. H. Lunsford, *J. Phys. Chem.***1986**, *90*, 4847–4851.
[30] R. A. Beyerlein, G. B. McVicker, L. N. Yacullo, J. J. Ziemak, *J. Phys. Chem.***1988**, *92*, 1967–1970.
[31] M. Gackowski, Ł. Kuterasiński, J. Podobiński, J. Datka, *ChemPhysChem***2018**, *19*, 3372–3379.
[32] P. V. Shertukde, W. K. Hall, J. M. Dereppe, G. Marcelin, *J. Catal.***1993**, *139*, 468–481.
[33] A. I. Biaglow, D. J. Parrillo, G. T. Kokotailo, R. J. A. Gorte, *J. Catal.***1994**, *148*, 213–223.
[34] R. Gounder, A. J. Jones, R. T. Carr, E. Iglesia, *J. Catal.***2012**, *286*, 214–223.
[35] Z. Qin, K. A. Cychosz, G. Melinte, H. El Siblani, J. P. Gilson, M. Thommes, C. Fernandez, S. Mintova, O. Ersen, V. Valtchev, *J. Am. Chem. Soc.***2017**, *139*, 17273–17276.
[36] S. M. T. Almutairi, B. Mezari, G. A. Filonenko, P. C. M. M. Magusin, M. S. Rigutto, E. A. Pidko, E. J. M. Hensen, *ChemCatChem***2013**, *5*, 452–466.
[37] I. Mirsojew, S. Ernst, J. Weitkamp, H. Knözinger, *Catal. Lett.***1994**, *24*, 235–248.
[38] L. M. Kustov, V. B. Kazansky, S. Beran, L. Kubelkova, P. Jiru, *J. Phys. Chem.***1987**, *91*, 5247–5251.
[39] P. Bazin, A. Alenda, F. Thibault-Starzyk, *Dalt. Trans.***2010**, *39*, 8432–8436.
[40] “SOD: Framework Type,” can be found under https://europe.iza-structure.org/IZA-SC/framework.php?STC=SOD.
[41] P. Sarv, T. Tuherm, E. Lippmaa, K. Keskinen, A. Root, *J. Phys. Chem.***1995**, *99*, 13763–13768.

[42] J. Kanellopoulos, C. Gottert, D. Schneider, B. Knorr, D. Prager, H. Ernst, D. Freude, *J. Catal.***2008**, *255*, 68–78.
[43] G. Li, E. A. Pidko, *ChemCatChem***2019**, *11*, 134–156.
[44] M. Sierka, J. Sauer, *J. Phys. Chem. B***2001**, *105*, 1603–1613.
[45] J. T. Fermann, *J. Chem. Phys.***2000**, *112*, 6787–6794.
[46] M. Hunger, *Rev. Sci. Eng.***1997**, *39*, 345–393.
[47] U. Eichler, M. Brandle, J. Sauer, *J. Phys. Chem. B***1997**, *101*, 10035–10050.
[48] S. Li, A. Zheng, Y. Su, H. Zhang, L. Chen, J. Yang, C. Ye, F. Deng, *J. Am. Chem. Soc.***2007**, *129*, 11161–11171.
[49] C. Schroeder, M. R. Hansen, H. Koller, *Angew. Chemie***2018**, *130*, 14477–14481.
[50] C. Schroeder, V. Siozios, C. Mück-Lichtenfeld, M. Hunger, M. R. Hansen, H. Koller, *Chem. Mater.***2020**, *32*, 1564–1574.
[51] C. P. Grey, A. J. Vega, *J. Am. Chem. Soc.***1995**, *117*, 8232–8242.
[52] O. Cairon, K. Thomas, T. Chevreau, *Microporous Mesoporous Mater.***2001**, *46*, 327–340.
[53] H. Awala, J.-P. Gilson, R. Retoux, P. Boullay, J. M. Goupil, V. Valtchev, S. Mintova, *Nat. Mat.***2015**, *14*, 447–451.

Table of Contents

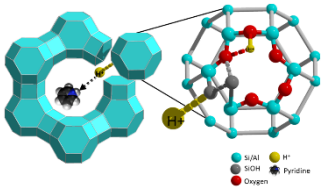

By combining advanced spectroscopies (IR and solid-state NMR) and molecular modeling, the present work reveals the presence of a proton transfer from the sodalite cage to the supercage of USY zeolite. When a basic probe molecule is in close proximity, the protonation is first assured by a “gate-keeper” silanol, which is restored by